








Identification of tqg flavor-changing neutral current interactions using machine learning techniques

Byeonghak Ko ,¹ Jeewon Heo ,¹ Woojin Jang ,¹ Jason S. H. Lee
,¹ Youn Jung Roh ,^{1,*} Ian James Watson ,¹ and Seungjin Yang ²

¹*Department of Physics, University of Seoul, Seoul 02504, Republic of Korea*

²*Department of Physics, Kyung Hee University, Seoul 02453, Republic of Korea*

Abstract

Flavor-changing neutral currents (FCNCs) are forbidden at tree level in the Standard Model (SM), but they can be enhanced in physics Beyond the Standard Model (BSM) scenarios. In this paper, we investigate the effectiveness of deep learning techniques to enhance the sensitivity of current and future collider experiments to the production of a top quark and an associated parton through the tqg FCNC process, which originates from the tug and tcg vertices. The tqg FCNC events can be produced with a top quark and either an associated gluon or quark, while SM only has events with a top quark and an associated quark. We apply machine learning techniques to distinguish the tqg FCNC events from the SM backgrounds, including qg -discrimination variables. We use the Boosted Decision Tree (BDT) method as a baseline classifier, assuming that the leading jet originates from the associated parton. We compare with a Transformer-based deep learning method known as the Self-Attention for Jet-parton Assignment (SAJA) network, which allows us to include information from all jets in the event, regardless of their number, eliminating the necessity to match the associated parton to the leading jet. The SAJA network with qg -discrimination variables has the best performance, giving expected upper limits on the branching ratios $Br(t \rightarrow qg)$ that are 25–35% lower than those from the BDT method.

Keywords: FCNC, top quark, Transformer-based, deep learning, self-attention, machine learning

*Electronic address: uosyoun14@uos.ac.kr

I. INTRODUCTION

Flavor-changing neutral currents (FCNCs) in the Standard Model (SM) are forbidden at the tree level and suppressed at higher orders through the Glashow–Iliopoulos–Maiani mechanism [1]. At the one-loop level of the SM, top quark FCNC branching ratios $Br(t \rightarrow ug)$ (respectively, $Br(t \rightarrow cg)$) are of the order of 10^{-14} (10^{-12}) [2]. However, FCNC interactions may enhance these branching ratios to up to 10^{-4} in scenarios including physics Beyond the Standard Model (BSM), such as the $Q = 2/3$ quark singlet model [3], the two Higgs doublet model [4], and the minimal supersymmetric Standard Model [5].

In this study, we focus on tqg FCNCs, where q is u or c , in proton–proton (pp) collisions at a center-of-mass energy of 13 TeV to probe BSM physics. The tree-level Feynman diagrams for the tqg FCNCs are shown in Figure 1, where the red dots indicate the tug and tcg vertices for tg production (Figure 1a) and tq production (Figure 1b). The tq production resembles SM events, while the tg production is forbidden at the tree level in the SM due to the conservation of charge and quark numbers. However, the proportion of tg production is

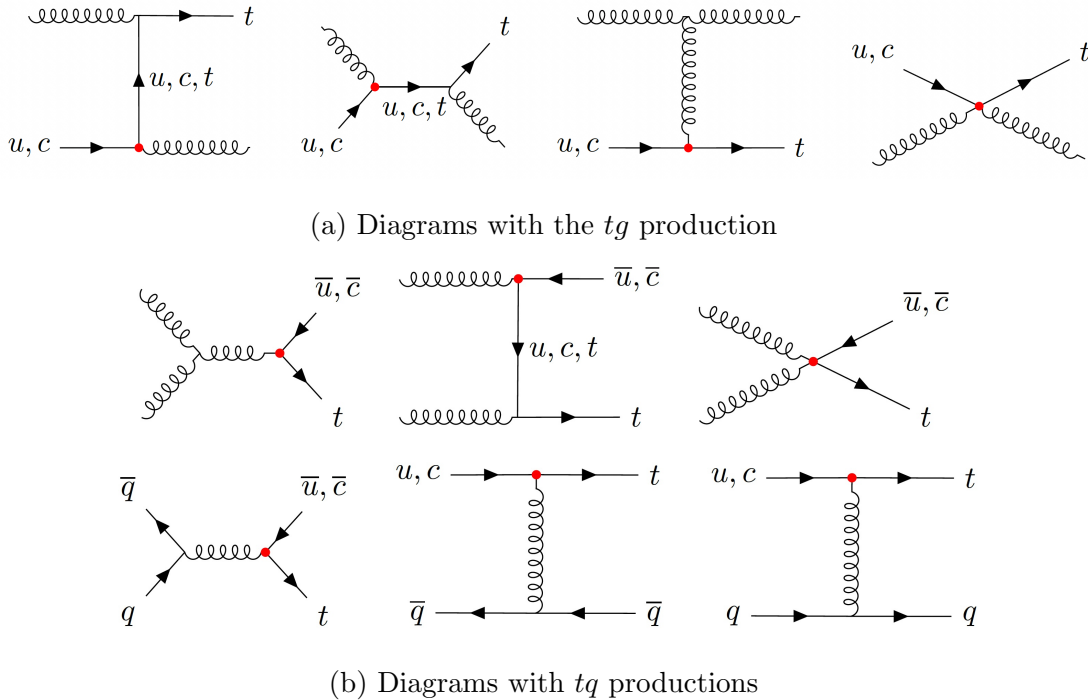


FIG. 1: The tree-level Feynman diagrams depicting the tqg FCNCs. The vertices that are colored red indicate the tug or tcg FCNC vertices in the diagram.

significantly higher than that of tq production, enabling us to distinguish tqg FCNC events from the SM.

Searches for tqg FCNCs have been performed by the ATLAS [6–8] and CMS [9] Collaborations in pp collisions at center-of-mass energies of 7, 8, and 13 TeV, and there is also a feasibility study to search for the tqg FCNC interactions in future colliders [10]. These studies used machine learning techniques with high-level features as inputs to produce their final results. However, they did not utilize gluon discrimination to enhance their sensitivity to the tqg FCNC interactions. In this study, we employ jet-based qg -discrimination variables [11–14] to distinguish the tqg FCNC events from the SM backgrounds.

We utilize the boosted decision trees (BDTs) as a baseline method for event classification [15]. We assign the leading jet as the jet originated from the associated parton, but the matching efficiency of the leading jet to the associated parton is approximately 60%. To improve over the baseline method by taking advantage of the full event topology, we adopt the Transformer-based deep learning method called the Self-Attention for Jet-parton Assignment (SAJA) network [16]. SAJA is able to utilize the information from all the jets in the event, regardless of the number of jets, thereby eliminating the need to match the associated parton to the leading jet.

II. SIMULATION

To simulate the signal events, we use the TOPFCNC model [17], which is an implementation of the tqg FCNC Lagrangian in the FEYNRULES package [18] in the universal FEYNRULES output format [19]. The effective Lagrangian terms involving the tqg FCNCs can be written as follows:

$$\frac{C_{qg}}{\Lambda^2} g_s \bar{t} \sigma^{\mu\nu} T^a q \tilde{\varphi} G_{\mu\nu}^a + \text{h.c.},$$

where Λ is the scale of the new physics, g_s is the coupling constant of the strong interaction, T^a are the generators of the $SU(3)$ gauge group, $G_{\mu\nu}^a$ is the gluon field strength tensor, and C_{qg} ($q = u, c$) is the strength of the tqg FCNC interaction. We set C_{qg}/Λ^2 as 0.2 TeV² for both $q = u, c$.

The tqg FCNC events in pp collision at 13 TeV are simulated using MADGRAPH 5 v2.6.7 [20] at the leading order (LO) with the 5-flavor scheme and the NNPDF 3.1 parton distribution function [21, 22]. The parton shower is performed using PYTHIA v8.224 [23] with

Monash 2013 tune [24]. The events contain at most two additional partons in the hard process, using the MLM scheme to merge the events [25]. We have observed that approximately 80% (50%) of events from tug (tcg) vertex have tg production. Detector simulation is carried out using DELPHES v3.4.2 [26] with the default CMS detector configuration card that comes with DELPHES.

We generate SM background events with the same simulation setup as the tqg FCNC signal samples. The samples we generate are the single top quark t-channel process, top quark pair production, and W +jets. Like FCNC processes, single top quark t-channel events have at most two additional partons in the hard process. Other potential backgrounds, such as single top quark processes associated with W bosons, Drell-Yan, and multijet backgrounds, are disregarded due to their comparatively negligible contributions after event selection.

III. EVENT SELECTION

The event topology of the tqg FCNC events is similar to the single top quark t-channel process. Therefore, we follow an event selection based on a recent CMS study, using Run II data, of the single top quark t-channel process, where the top quark decays leptonically [27]. We select muons and electrons with $p_T > 30$ GeV, $|\eta| < 2.4$, and isolation < 0.06 , using a relative particle flow isolation with $\Delta R < 0.4$ (0.3) for muons (electrons) [28]. We discard events with any additional lepton with $p_T > 15$ GeV, $|\eta| < 2.4$, and isolation < 0.20 .

Jets are reconstructed from the particle flow outputs using the anti- k_T algorithm [29] with a cone size of $\Delta R = 0.4$ as implemented in FASTJET v3.3.2 [30]. We select jets with $p_T > 40$ GeV and $|\eta| < 2.4$. We reject jets where the ΔR between the jet and the selected lepton is smaller than 0.4. We simulate b -jet tagging, following the b -tagging efficiency and mistag rates from the CMS CSVv2 medium working point [31, 32], by updating the parameterized b -jet tagging efficiency and mistag rates in the DELPHES card. We select events with at least two jets and require that events have at least one b -tagged jet.

We define the transverse W mass as the transverse mass of the reconstructed lepton and the reconstructed missing transverse momentum, \vec{p}_T^{miss} . We reject events where the transverse W mass is smaller than 50 GeV to suppress multijet background events.

We reconstruct the top quark from the selected lepton, b -jet, and \vec{p}_T^{miss} using a method based on the previous tqg FCNC search by CMS [9]. We assume that \vec{p}_T^{miss} corresponds to

the neutrino \vec{p}_T and we estimate the component p_z of the neutrino momentum along the beam direction by requiring the lepton and neutrino give the W boson mass $M_W = 80.4$ GeV [33], which leads to a quadratic equation whose solution is p_z . In the case of real solutions, the smallest value is taken as p_z . If the solutions are complex, we modify \vec{p}_T^{miss} to make the transverse W mass equal to M_W to eliminate the imaginary part of the solution. The modified \vec{p}_T^{miss} is used only for the top quark reconstruction.

IV. ANALYSIS STRATEGY

A previous search for tqg FCNCs performed by the CMS Collaboration [9] used only the kinematic and event topology variables listed in Table I. The variables used are the kinematic variables of the reconstructed top quark and the leading jet and event topology variables such as opening angles in the W boson and the top quark rest frames. Figure 2 displays kinematic distributions of the reconstructed top quark and the leading jet from tqg FCNC events and SM backgrounds.

The higher color factor of gluons compared to quarks results in gluon jets generally having more jet constituents, broader shape, and softer fragmentation compared to quark jets. The CMS Collaboration has performed studies of qg -discrimination using the multiplicity of jet constituents, major (minor) axes $\sigma_M(j)$ ($\sigma_m(j)$) of jets in the $\eta - \phi$ space, and jet energy sharing $p_T D = \frac{\sqrt{\sum p_{T,i}^2}}{\sum p_{T,i}}$, where i indexes over jet constituents, as inputs [11, 12]. Further studies suggest splitting the total multiplicity to the individual numbers of charged hadrons, neutral hadrons, electrons, muons, and photons [13, 14]. The qg -discrimination variables used in this paper are listed in Table II, and Figure 3 shows their distributions.

The impact of the qg -discrimination variables is evaluated by comparing two BDTs. The first BDT is constructed with variables listed in Table I, and the other one is constructed with variables in both Table I and II. We train BDTs to discriminate tqg FCNC signal from SM backgrounds. We use Toolkit for Multivariate Data Analysis (TMVA) v.4.3.0, which is a part of the ROOT framework, to implement the BDTs with AdaBoost [34–36]. The parameters used for the BDTs are listed in Table III. During BDT training, we weight the background events such that each background sample is normalized to its cross-section. Additionally, we scale the total background weights to match the number of signal events. We have four BDTs. The tug and tcg signal samples are separately trained with a model

that uses the input variables listed in only Table I as the baseline, and another model that includes the baseline variables and qg -discrimination variables in Table II for the leading jet.

In the BDT setup, we assume that the leading jet (i.e., the most energetic jet which is not b -tagged) comes from the associated parton. After the event selection, the associated parton is the leading jet in 60% of events, using $\Delta R < 0.3$ to match jets to partons. Unmatched partons are primarily due to initial state radiation, mistagging the b -jet from the top quark decay, or gluon splitting. As the BDT model takes in a fixed number of inputs, and cannot adapt to varying numbers of jets, we use only the leading jet variables in this study. This

Variables	Definition
$\eta(l)$	Pseudorapidity of the lepton
$p_T(j_L)$	Transverse momentum of the leading light jet
$\eta(j_L)$	Pseudorapidity of the leading light jet
$p_T(b)$	Transverse momentum of the leading b -tagged jet
$p_T(j_1)$	Transverse momentum of the leading jet
$\text{sgn}(l)$	Charge of the lepton
$H_T(j_1, j_2)$	The scalar sum of p_T of the leading jet and the sub-leading jet
$p_T(j_1, j_2)$	The vector sum of p_T of the leading jet and the sub-leading jet
$m(j_1, j_2)$	The invariant mass of the leading jet and the sub-leading jet
$m(W + \sum j)$	The invariant mass of the W boson and jets
$p_T(t)$	Transverse momentum of the top quark
$m(t)$	The mass of top quark
Planarity	The smallest eigenvalue of a tensor $(\sum_{\alpha} p_{\alpha}^i p_{\alpha}^j) / (\sum_{\alpha} (p_{\alpha})^2)$, where the summations run over jets, the lepton and \vec{p}_T^{miss}
$\cos \theta(l, j)_{\text{top}}$	Opening angle of the lepton and the leading light jet in the top quark rest frame
$\cos \theta(l, W)_W$	Opening angle of the lepton and the W boson direction in the W boson rest frame
$\cos \theta(W, j)_{\text{top}}$	Opening angle of the W boson and the leading light jet in the top quark rest frame

TABLE I: The input variables of the BDT. This includes information from the lepton, the missing transverse momentum, the leading jet, the leading b -tagged jet, the W boson, and the top quark.

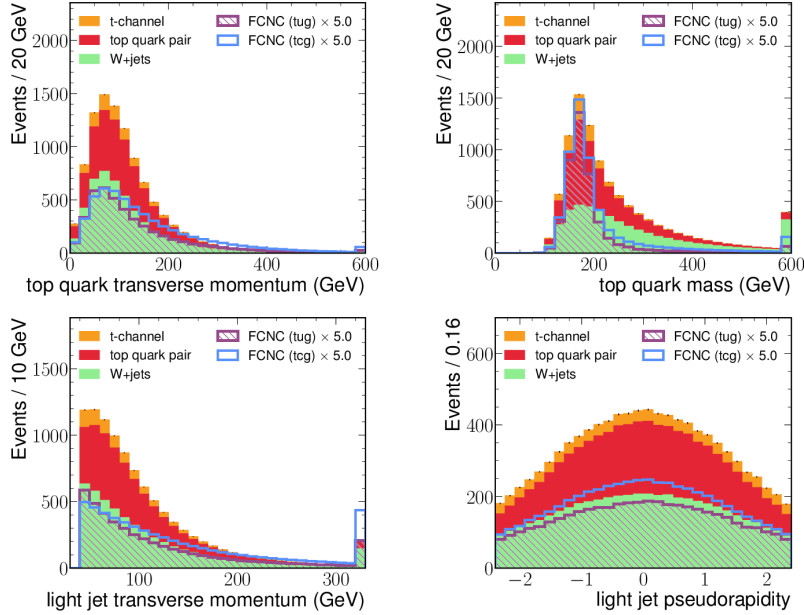


FIG. 2: Distributions of reconstructed top quark kinematics and leading jet kinematics for the tqg FCNC events and SM backgrounds. These variables are used as the input variables of the BDT and SAJA. The total background statistical uncertainty is displayed by the black vertical lines. The distributions of tug and tcg FCNC events are drawn 5 times larger. The distributions are scaled to an integrated luminosity 138 fb^{-1} .

limits the performance of the BDT due to the misidentification of the associated parton. As an alternative approach which solves this issue, we adopt the deep learning model SAJA which can take an arbitrary number of jets as input.

SAJA is a Transformer-based model [37] which consists mainly of feed-forward networks and multi-head self-attention blocks. The original SAJA model is designed to match jets to partons, so it only takes jets as inputs. In this analysis, however, we extend the input objects to include the lepton and the missing transverse momentum as well as jets. For this purpose, we allocate an encoder, defined as a feed-forward network, to each input physics object, which takes the object's input variables to a vector of a common size. The dimensions of the input vectors corresponding to each object are $D_{\text{Lepton}} = 6$, $D_{\text{MET}} = 2$, and $D_{\text{Jet}} = 13$ when the qg -discrimination variables are used, otherwise $D_{\text{Jet}} = 5$ (per Table II and V). The output of the encoders is concatenated and fed into a sequence of multi-head self-attention blocks. All operations have the same output dimension, denoted as D_{model} , except the output dimension of the first affine transformation in all feed-forward networks, denoted as

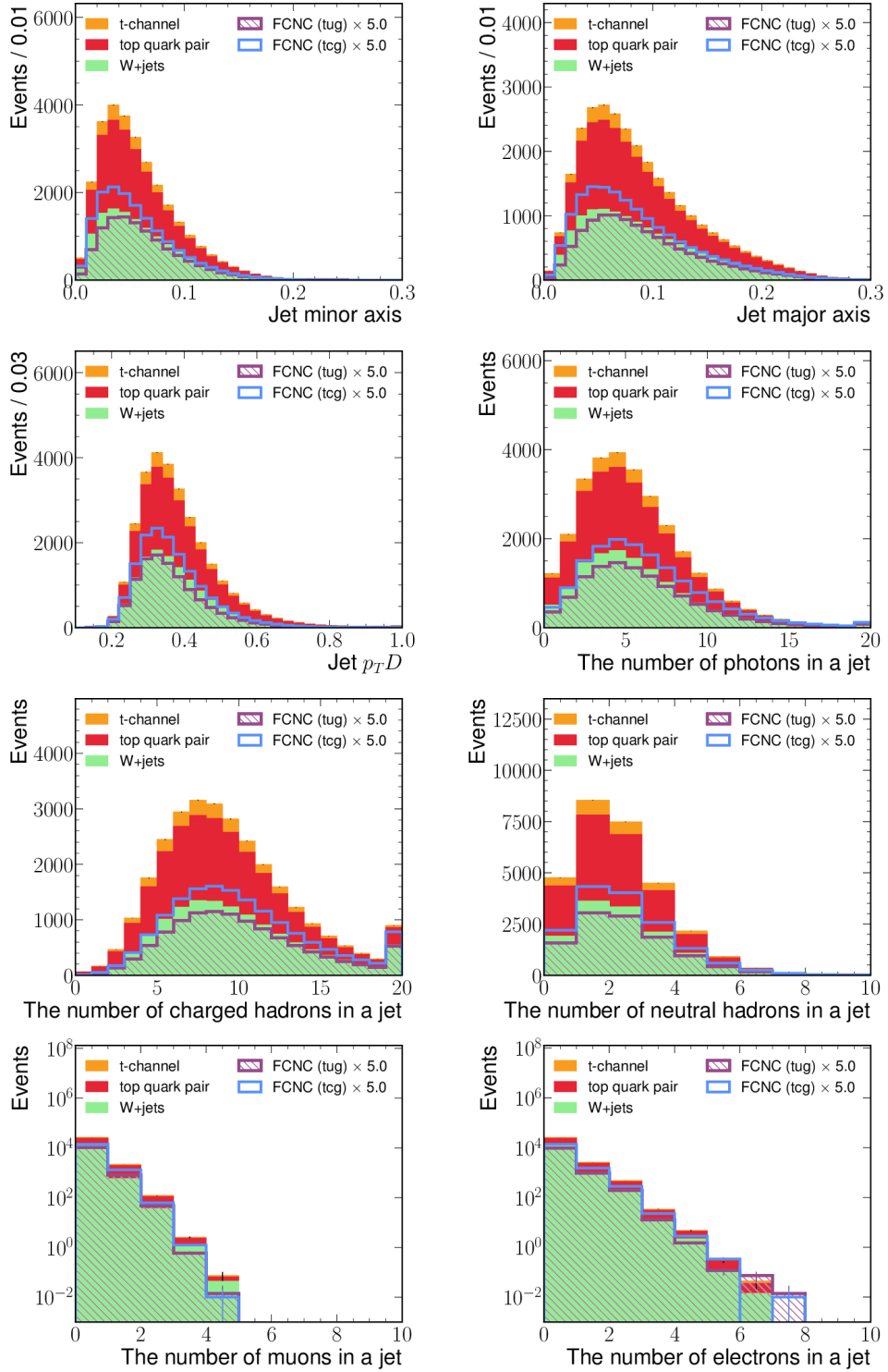


FIG. 3: Distributions of the qq -discrimination variables for the tqg FCNC events and SM backgrounds. These variables are used as the input variables of the BDT and SAJA. The total background statistical uncertainty is displayed by the black vertical lines. The distributions of tug and tcg FCNC events are drawn 5 times larger. The distributions are scaled to an integrated luminosity 138 fb^{-1} .

Variables	Definition
$N_{h\pm}(j)$	The number of charged hadrons in jet j
$N_{h0}(j)$	The number of neutral hadrons in jet j
$N_e(j)$	The number of electrons in jet j
$N_\mu(j)$	The number of muons in jet j
$N_\gamma(j)$	The number of photons in jet j
$\sigma_M(j), \sigma_m(j)$	The major and minor axes of jet j in the $\eta - \phi$ space
$p_T D(j)$	$\sqrt{\sum_i (p_{T,i})^2} / \sum_i p_{T,i}$ (i is indexed over the jet constituents)

TABLE II: The qg -discrimination variables that are input into the machine learning models. The variables are taken from [14].

Name	Description	Value
AdaBoostBeta	Learning rate for AdaBoost algorithm	0.5
nCuts	Number of grid points in variable range used in finding optimal cut in node splitting	20
NTrees	Number of trees in the forest	850
MinNodeSize	Minimum percentage of training events required in a leaf node	2.5%
MaxDepth	Max depth of the decision tree allowed	3
BaggedSampleFraction	Relative size of bagged event sample to original size of the data sample	0.5

TABLE III: The hyperparameters of all BDTs. The variable names and the descriptions are from the TMVA manual [34]

$D_{\text{feedforward}}$. The structure of SAJA in this study is depicted in Figure 4.

The output of the original SAJA model is jet-wise scores of assignment to partons, so the original model has jet-wise feed-forward networks and softmax after the self-attention blocks. Since our model is designed to classify tqg FCNC events from SM backgrounds, we construct a single event latent vector by taking the mean along the object axis and take one feed-forward network followed by a sigmoid $\frac{1}{1+e^{-x}}$ giving a classification score between 0 and 1 as the model output.

We consider five hyperparameters for SAJA, $D_{\text{feedforward}}$, D_{model} , the number of heads, the number of blocks in the sequence of self-attention blocks, and the dropout [38] rate. The

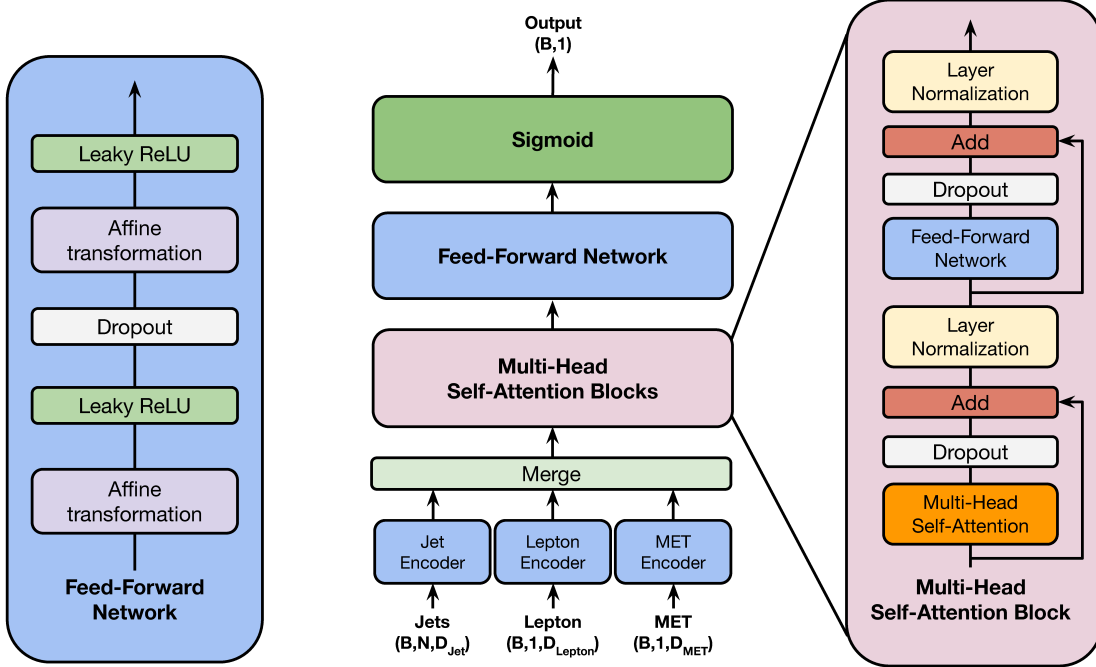


FIG. 4: Diagram showing the data flow of the SAJA model used in this study, where B is the batch size, N is the number of jets and D_{Jet} , D_{Lepton} , D_{MET} are the number of input variables of each jet, the lepton, and the missing transverse momentum, respectively.

These number are determined by the number of input variables in Table II and V.

specific values for these hyperparameters are listed in Table IV. We use Adam optimization algorithm [39], where the learning rate is set to 0.0003, $\beta_1 = 0.9$, and $\beta_2 = 0.999$. For both BDT and SAJA, we separate tqg FCNC events and SM backgrounds into the training dataset (64%), test dataset (20%), and validation dataset (16%). When training each model, we use the same training, test, and validation datasets. During training, we weight the background events as in the BDT case. As for the case of the BDT training, tug and tcg are trained separately with a baseline input variable model (listed in Table V for SAJA) and a model including qg -discrimination variables (Table II). Since SAJA can combine the information from the individual input objects through the self-attention layers to produce a representation which can be efficiently used for event classification, the input variables for SAJA are only the physics object-related variables, whereas the BDT variables include composite variables, like the reconstructed top quark mass and planarity.

Name	Value
$D_{\text{feedforward}}$	256
D_{model}	160
The number of heads	10
The number of self-attention blocks	2
Dropout rate	0.1

TABLE IV: The hyperparameters of all SAJA networks

Variables	Definition
$p_T(j), \eta(j), \phi(j), m(j)$	Kinematic variables of each jet
f_b	A variable with value 1 (0) if the jet is (is not) b -tagged
$p_T(l), \eta(l), \phi(l), m(l)$	Kinematic variables of the lepton
$\text{sgn}(l)$	Charge of the lepton
muon bit	A variable with value 1 (0) if the lepton is muon (electron)
$E_T^{\text{miss}}, \phi(\vec{p}_T^{\text{miss}})$	Magnitude and azimuthal angle of \vec{p}_T^{miss}

TABLE V: The input variables of the SAJA network. This includes the information on the lepton, missing transverse momentum, and all jets in the event.

V. RESULTS

The output distributions of the BDTs and SAJA networks, obtained from the test dataset, are displayed in Figure 5 and Figure 6. For each of the output distributions, we construct the receiver operating characteristic (ROC) curve and the significance improvement characteristic (SIC) [40] as a function of the signal efficiency. The SIC is defined as $\epsilon_S/\sqrt{\epsilon_B}$, where ϵ_S is the signal efficiency and ϵ_B is the background efficiency. We compare the methods by integrating the ROC curve to get the area under the curve (AUC) and by finding the maximum SIC.

The ROC and SIC curves for each method, along with the values of AUC and maximum SIC, are shown in Figure 7. The results are shown using signal samples originating from tug vertex (Figure 7a and 7b) and tcg vertex (Figure 7c and 7d) separately. The blue dashed lines represent the baseline BDT performance. By including the qg -discrimination

Type		95% CL upper limit on $Br(t \rightarrow qq)$
tug	BDT	6.73×10^{-6}
	BDT+ qq -disc	6.38×10^{-6}
	SAJA	5.61×10^{-6}
	SAJA+ qq -disc	5.01×10^{-6}
tcg	BDT	5.89×10^{-6}
	BDT+ qq -disc	5.69×10^{-6}
	SAJA	4.40×10^{-6}
	SAJA+ qq -disc	3.83×10^{-6}

TABLE VI: The 95% CL upper limit on $Br(t \rightarrow ug)$ and $Br(t \rightarrow cg)$ by BDT without qq -discrimination variables and SAJA with qq -discrimination variables

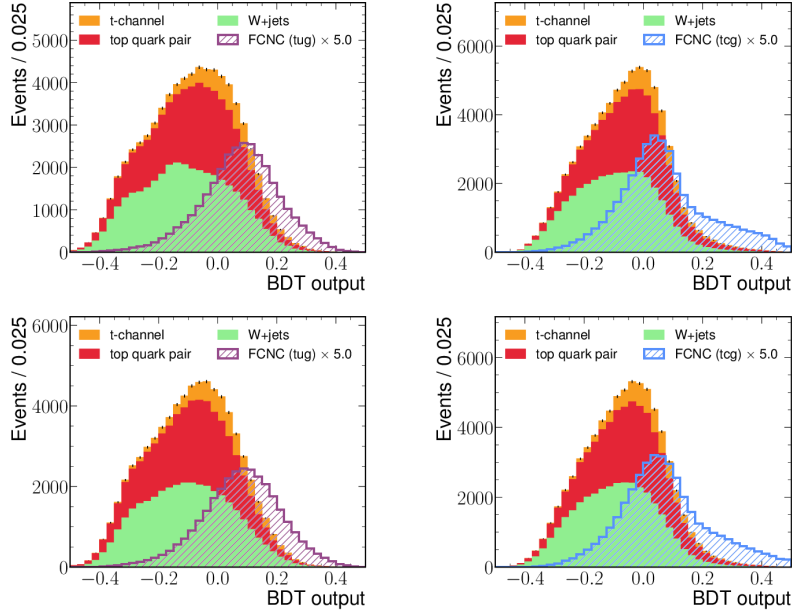


FIG. 5: The output distribution of BDTs obtained from the test dataset. The left (right) columns are from the training with tug (tcg) signal samples. The networks for the top row use the baseline input variables, and those for the bottom row add the qq -discrimination variables. The total background statistical uncertainty is displayed by the black vertical lines.

variables in the BDT, the blue solid line, we observe slight increases in both the AUC and the maximum SIC compared to the baseline. The SAJA network without qg -discrimination variables, shown in the red dashed lines, significantly outperforms both BDTs for all signal efficiencies in both ROC and SIC. Adding qg -discrimination variables to the SAJA network, as shown in the red lines, improves the performance, like the BDT case, but the improvement for SAJA is much more significant and results in the best overall performance.

We calculate the 95% CL upper limits on $Br(t \rightarrow qg)$ ($q = u, c$) to assess the impact on physics of our findings. We choose events according to the threshold giving the maximum SIC for each model. To find the expected upper limits, we assume the observation of the background-only hypothesis, with B events, and find the number of signal events S , where the lower tail integral, up to B , of the Gaussian centered at $S + B$ with width $\sqrt{S + B}$ is 5%, which is then translated into an upper limit on the signal cross section. Utilizing the fact that the signal cross section is proportional to C_{qg}^2 , we derive the 95% CL upper limits on C_{qg}^2 . Finally, we determine the upper limits on $Br(t \rightarrow qg)$ by employing the known relationship between C_{qg} and $Br(t \rightarrow qg)$ [41]. The expected upper limits from all methods are listed in Table VI assuming an integrated luminosity equivalent to the Run 2 of the LHC, 138 fb^{-1} . The expected upper limits on $Br(t \rightarrow qg)$ by SAJA with qg -discrimination variables are 25% and 35% lower than the upper limits by the BDT baseline.

VI. CONCLUSION

We investigate the effectiveness of using deep learning methods to enhance the sensitivity of collider searches for the tqg FCNC process. To enhance the distinction between the tqg FCNC signals and SM backgrounds, we utilize qg -discrimination variables and introduce the SAJA network to incorporate objects including all jets and the complete event topology. Our study shows that the SAJA network outperforms the BDT baseline, and with the addition of qg -discrimination variables, SAJA makes further improvements. The performance is evaluated by the expected 95% CL upper limits on the branching ratios $Br(t \rightarrow ug)$ and $Br(t \rightarrow cg)$, where the branching ratios obtained by SAJA network with the qg -discrimination variables is 25% and 35% lower than those by BDT.

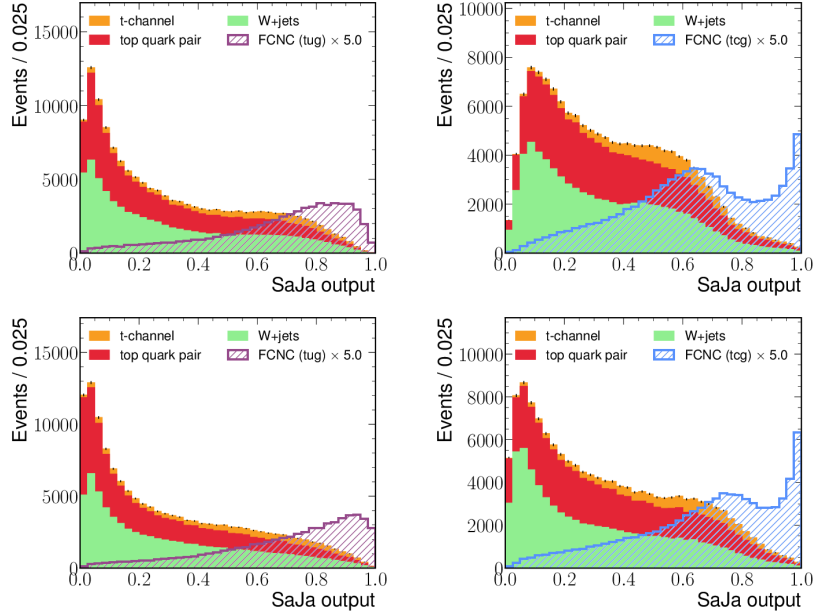


FIG. 6: The output distribution of SAJA networks obtained from the test dataset. The left (right) columns are from the training with tug (tcg) signal samples. The networks for the top row use the baseline input variables, and those for the bottom row add the gg -discrimination variables. The total background statistical uncertainty is displayed by the black vertical lines.

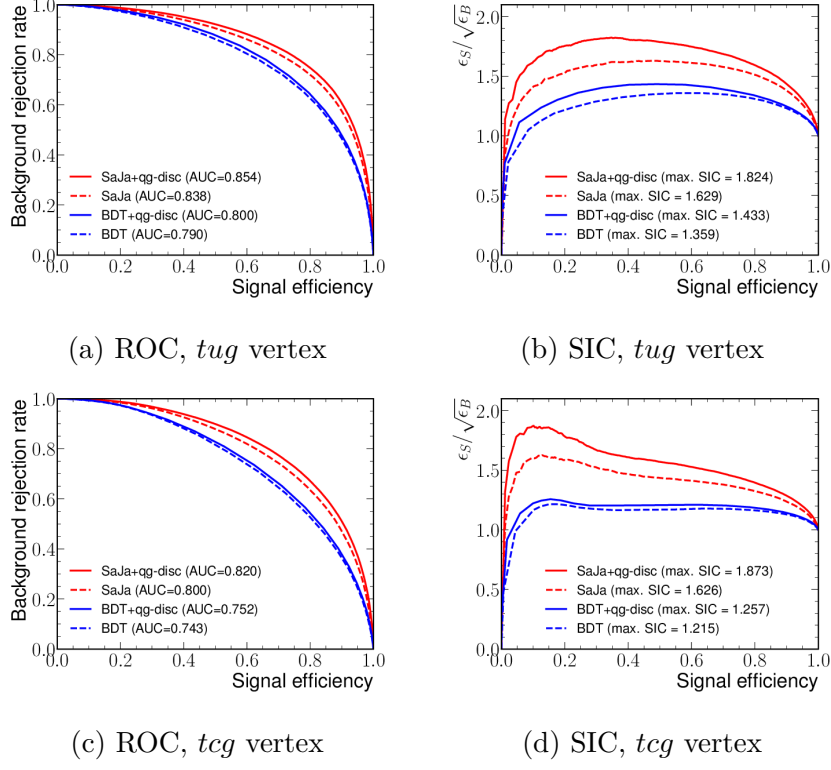


FIG. 7: The ROC curves (left column) and the SIC curves (right column) from BDT and SAJA. The models are trained with signals having the *tug* vertex (a, b) and the *tcg* vertex (c, d). We use BDT (blue line) and SAJA (red line) and train with *qq*-discrimination variable (solid line) and without *qq*-discrimination variable (dashed line). Max. SIC means the maximum value of $\epsilon_S/\sqrt{\epsilon_B}$.

Acknowledgments

This work was supported by the National Research Foundation of Korea (NRF) grant funded by the Korea government (MSIT). (No. 2021R1A2C1093704). This research was supported by Basic Science Research Program through the National Research Foundation of Korea (NRF) funded by the Ministry of Education (2018R1A6A1A06024977). This work was supported by the National Research Foundation of Korea (NRF) grant funded by the Korea government (MSIT). (No. 2018R1C1B6005826). This work was supported by the National Research Foundation of Korea (NRF) grant funded by the Korea government (MSIT). (No. 2023R1A2C2002751). This work was supported by the 2022 sabbatical year research grant of the University of Seoul.

-
- [1] S. L. Glashow, J. Iliopoulos, and L. Maiani, *Phys. Rev. D* **2**, 1285 (1970)
<https://doi.org/10.1103/PhysRevD.2.1285>.
 - [2] J. A. Aguilar-Saavedra, *Acta Phys. Polon. B* **35**, 2695 (2004).
 - [3] J. A. Aguilar-Saavedra, *Phys. Rev. D* **67**, 035003 (2003)
<https://doi.org/10.1103/PhysRevD.67.035003>.
 - [4] F. del Aguila, J. A. Aguilar-Saavedra and R. Miquel, *Phys. Rev. Lett.* **82**, 1628 (1999)
<https://doi.org/10.1103/PhysRevLett.82.1628>.
 - [5] J. Guash and J. Sola, *Nucl. Phys. B* **562**, 3 (1999)
[https://doi.org/10.1016/S0550-3213\(99\)00579-9](https://doi.org/10.1016/S0550-3213(99)00579-9).
 - [6] ATLAS Collaboration, *Eur. Phys. J. C* **82**, 334 (2022)
<https://doi.org/10.1140/epjc/s10052-022-10182-7>.
 - [7] ATLAS Collaboration, *Eur. Phys. J. C* **76**, 55 (2016)
<https://doi.org/10.1140/epjc/s10052-016-3876-4>.
 - [8] ATLAS Collaboration, *Phys. Lett. B* **712**, 351 (2012)
<https://doi.org/10.1016/j.physletb.2012.05.022>.
 - [9] CMS Collaboration, *JHEP* **02**, 028 (2017)
<https://doi.org/10.1007/JHEP02%282017%29028>.
 - [10] K. Y. Oyulmaz, A. Senol, H. Denizli, and O. Cakir, *Phys. Rev. D* **99**, 115023 (2019)

- <https://doi.org/10.1103/PhysRevD.99.115023>.
- [11] CMS Collaboration, CMS-PAS-JME-13-002 (2013).
- [12] T. Cornelis et al., arXiv:1409.3072 (2014).
- [13] J. S. H. Lee et al., J. Korean Phys. Soc. **74**, 219 (2019)
<https://doi.org/10.3938/jkps.74.219>.
- [14] J. S. H. Lee et al., J. Korean Phys. Soc. **75**, 652 (2019)
<https://doi.org/10.3938/jkps.75.652>.
- [15] J. H. Friedman, The Annals of Statistics, Vol. **29**, No. 5, pp. 1189-1232 (2001)
<http://dx.doi.org/10.1214/aos/1013203451>.
- [16] J. S. H. Lee, I. Park, I. J. Watson, and S. Yang, J. Korean Phys. Soc. **84**, 427-438 (2024)
<https://doi.org/10.1007/s40042-024-01037-3>.
- [17] C. Degrande, F. Maltoni, J. Wang and C. Zhang, Phys. Rev. D **91**, 034024 (2015)
<https://doi.org/10.1103/PhysRevD.91.034024>.
- [18] A. Alloul et al., Comput. Phys. Commun. **185** 2250 (2014)
<https://doi.org/10.1016/j.cpc.2014.04.012>.
- [19] C. Degrande et al., Comput. Phys. Commun. **183** 1201 (2012)
<https://doi.org/10.1016/j.cpc.2012.01.022>.
- [20] J. Alwall et al., JHEP **1407**, 079 (2014)
<https://doi.org/10.1007/JHEP07%282014%29079>.
- [21] A. Buckley et al., Eur. Phys. J. C **75**, 3, 132 (2015)
<https://doi.org/10.1140/epjc/s10052-015-3318-8>.
- [22] NNPDF Collaboration, Eur. Phys. J. C **77**, 10, 663 (2017)
<https://doi.org/10.1140/epjc/s10052-017-5199-5>.
- [23] T. Sjöstrand et al., Comput. Phys. Commun. **191**, 159 (2015)
<https://doi.org/10.1016/j.cpc.2015.01.024>.
- [24] P. Skands, S. Carrazza and J. Rojo, Eur. Phys. J. C **74** 8, 3024 (2014)
<https://doi.org/10.1140/epjc/s10052-014-3024-y>.
- [25] M. L. Mangano, et al., JHEP **01**, 013 (2007)
<https://doi.org/10.1088/1126-6708/2007/01/013>.
- [26] J. de Favereau et al., JHEP **02**, 57 (2014)
<https://doi.org/10.1007/JHEP02%282014%29057>.

- [27] CMS Collaboration, Eur. Phys. J. C **80** 370, (2020)
<https://doi.org/10.1140/epjc/s10052-020-7858-1>.
- [28] CMS Collaboration, Phys. Lett. B **713**, 2, 68-90 (2012)
<https://doi.org/10.1016/j.physletb.2012.05.028>.
- [29] M. Cacciari, G. P. Salam and G. Soyez, JHEP **0804**, 063 (2008)
<https://doi.org/10.1088/1126-6708/2008/04/063>.
- [30] M. Cacciari, G. P. Salam and G. Soyez, Eur. Phys. J. C **72**, 1896 (2012)
<https://doi.org/10.1140/epjc/s10052-012-1896-2>.
- [31] CMS Collaboration, JINST **8**, P04013 (2013)
<https://doi.org/10.1088/1748-0221/8/04/P04013>.
- [32] CMS Collaboration, A. M. Sirunyan et al., JINST **13**, P05011 (2018)
<https://doi.org/10.1088/1748-0221/13/05/P05011>.
- [33] Particle Data Group, K. A. Olive et al., Review of Particle Physics, Chin. Phys. C **38**, 090001 (2014) <https://doi.org/10.1088/1674-1137/38/9/090001>.
- [34] J. Therhaag [TMVA Core Developer Team], AIP Conf. Proc. **1504**, 1013 (2009)
<https://doi.org/10.1063/1.4771869>.
- [35] A. Hoecker et al., CERN-OPEN-2007-007 (2007).
- [36] R. Brun and F. Rademakers, Nucl. Inst. & Meth. in Phys. Res. A **389**, 81-86 (1997)
[https://doi.org/10.1016/S0168-9002\(97\)00048-X](https://doi.org/10.1016/S0168-9002(97)00048-X).
- [37] A. Vaswani, N. Shazeer, N. Parmar, J. Uszkoreit, L. Jones, A. N. Gomez, L. Kaiser, and I. Polosukhin, <http://arxiv.org/abs/1706.03762>.
- [38] G. E. Hinton, N. Srivastava, A. Krizhevsky, I. Sutskever and R. R. Salakhutdinov,
<http://arxiv.org/abs/1207.0580>.
- [39] D. P. Kingma and J. Ba, <https://arxiv.org/abs/1412.6980>.
- [40] K. Black et al., JHEP **04**, 069 (2011)
[https://doi.org/10.1007/JHEP04\(2011\)069](https://doi.org/10.1007/JHEP04(2011)069).
- [41] G. Durieux, F. Maltoni and C. Zhang, Phys. Rev. D **91**, 074017 (2015)
<https://doi.org/10.1103/PhysRevD.91.074017>.